Int. J. Heat Mass Transfer. Vol. 27, No. 6, pp. 799–813, 1984
Printed in Great Britain

0017 9310/84 $3.00 + 0.00

COMBINED NATURAL AND FORCED CONVECTION IN A HORIZONTAL POROUS CHANNEL

M. HAAJIZADEH and C. L. TIEN
Department of Mechanical Engineering, University of California, Berkeley, CA 94720, U.S.A.

(*Received* 18 *January and in revised form* 28 *June* 1983)

Abstract—In this paper, combined natural and forced convective flows through a horizontal porous channel connecting two reservoirs have been investigated both analytically and numerically. The forced throughflow is induced by an end-to-end mean pressure difference, while the natural convective motion is driven by a horizontal temperature gradient. The solutions are governed by three dimensionless parameters: the Rayleigh number R, based on permeability, the channel aspect ratio L (length/height) and the dimensionless end-to-end pressure difference P, equivalent of the Peclet number. For small R, fixed L and $P = O(1)$, an asymptotic expression based on the regular perturbation analysis is established for the Nusselt number up to $O(R^2)$ as $R \to 0$. For fixed R and $P = O(1/L)$ solutions for long channels, $L \to \infty$, are found by using matched asymptotic expansions, and the Nusselt number is evaluated up to $O(1/L^3)$. Finally, the numerical solutions of the full governing equations are obtained by the finite-difference successive over-relaxation technique. These solutions cover the parameter range $R \leqslant 80$, $2 \leqslant L \leqslant 5$ and $0 \leqslant P/R \leqslant 0.5$. A comparison with the numerical solutions shows that the asymptotic solutions are valid for the parameter range of $(R^2/L^3) \lesssim 50$ and $P \lesssim 1.5$. For this range the results indicate that heat transfer enhancement due to the natural convection and the forced flow can be simply added together in spite of the non-linear interaction of these two fields. The results also show that even a small rate of throughflow has a significant effect on the temperature distribution and the heat transfer across the channel, and for $P/R \gtrsim 0.2$ the contribution of the natural convection to the Nusselt number is negligible.

NOMENCLATURE

a	constant
$C_0, C_1, C_2, \ldots$	core-flow parameters
$D_0, D_1, D_2, \ldots$	core-flow parameters
g	gravitational acceleration
h	height
i	dummy index
l	length
L	aspect ratio, l/h
m	dummy index
$\dot{m}$	dimensionless throughflow rate, equation (8)
n	dummy index
N	Nusselt number
N_a	asymptotic Nusselt number, equation (53)
N_c	cold-side average temperature gradient
N_f	pure forced-convection Nusselt number
N_h	hot-side average temperature gradient
P	dimensionless end-to-end mean pressure difference equivalent to the Peclet number, $\kappa(p_h - p_c)/\mu\alpha$
p	dimensionless pressure
p_c	cold-side mean pressure
p_h	hot-side mean pressure
Q	any dimensionless variable, u, v, p, T or Ψ
Q^*	core variables in terms of inner coordinate near cold side
R	Rayleigh number based on permeability, $\beta g h \kappa (T_h - T_c)/\nu\alpha$
S	constant
T	dimensionless temperature
T_c	cold-side temperature
T_f	temperature pertaining to pure forced convection
T_h	hot-side temperature
u, v	dimensionless horizontal and vertical velocities
x, y	horizontal and vertical distances.

Greek symbols

α	effective thermal diffusivity
β	thermal expansion coefficient of the fluid
δ, ε	criteria for numerical convergence
η	heat transfer enhancement due to the natural convection, equation (60)
κ	permeability
μ	absolute viscosity
ν	kinematic viscosity
ρ_c	fluid density at T_c
σ	criterion for numerical convergence
ϕ	dimensionless mean pressure difference scaled by R, equation (9)
ψ	dimensionless stream function
ω	dimensionless pressure difference, PL.

Subscripts

c	cold reservoir
f	pure forced convection
h	hot reservoir
max	maximum
0, 1, 2, ...	zero, first, second, ..., order approximations for $L \to \infty$
$(\,)_{x=0}$	at $x = 0$

Superscripts

$\bar{}$ core region

$\tilde{}$ cold-end region

$\hat{}$ hot-end region

$'$ dimensional quantities

$(0),(1),(2),\ldots$ zero, first, second, ..., order solutions for $R \to 0$.

Other notation

H.O.T. higher order terms.

1. INTRODUCTION

IN A PREVIOUS study, Bejan and Tien [1] considered natural convection in a horizontal porous layer connecting two fluid reservoirs. The driving force in their study was the temperature difference between the reservoirs, which induced a natural counterflow in the layer. They showed that the end-wall permeability yields higher heat transfer rates due to the direct fluid communication with the reservoirs. In many practical situations, however, there may be a mean pressure difference through the layer, which would superimpose a forced flow on the natural counterflow considered in ref. [1]. Incorporation of this pressure difference is worthy of consideration, since even a small throughflow rate affects the flow structure and the total heat transfer significantly. In the present study analytical and numerical solutions are presented for this combined natural and forced convection problem.

In the light of frequent occurrence in various physical systems, the phenomenon of combined natural and forced convection in porous media has been the subject of many recent studies. Of particular engineering interest are those convection problems found in geothermal systems where pressure gradients are generated as a result of geothermal fluids withdrawal and reinjection, or hydrostatic pressure imbalance due to the variations of the water-table level; in packed bed reactors where reactants are injected and products removed; in thermal oil recovery where the processes involve the flow of heated fluids; and in thermal insulations where the internal and external hydrostatic pressure imbalance generates leakage velocities. Most of the previous studies on this phenomenon have been focused on the effect of throughflows on the natural convection in a horizontal porous layer induced by a vertical temperature gradient [2–6]. In contrast, there appears very limited studies on the interaction mechanism between a throughflow and a flow driven by a horizontal temperature gradient [7], although interactions of this type are very common in the above-mentioned engineering systems. Indeed few studies have been reported on the corresponding combined natural and forced convection in a horizontal channel filled with an incompressible fluid [8].

In Section 2 the governing equations for the problem are stated. The subsequent sections treat the problem by perturbation theory in the limits of low Rayleigh numbers and long narrow channels, respectively. These solutions are then compared with the numerical solutions of the full governing field equations obtained by the finite-difference successive over-relaxation technique.

2. FORMULATION OF THE PROBLEM

The model, Fig. 1, consists of a horizontal porous channel connecting two reservoirs. The vertical permeable boundaries of height h are assumed to be maintained at the corresponding constant reservoir temperatures T_c and T_h ($T_c < T_h$), and under the hydrostatic pressure of the adjacent reservoirs. The permeable horizontal boundaries of length l are insulated. The flow is assumed to be steady and two-dimensional (2-D). Invoking Darcy's law along with the Boussinesq approximation and neglecting thermal dispersion, the governing equations and boundary conditions are

$$\partial u/\partial x + \partial v/\partial y = 0, \tag{1}$$

$$u = -\partial p/\partial x, \tag{2}$$

$$v = -\partial p/\partial y + RT, \tag{3}$$

$$u\,\partial T/\partial x + v\,\partial T/\partial y = \partial^2 T/\partial x^2 + \partial^2 T/\partial y^2, \tag{4}$$

$$\left.\begin{aligned} &p = -P, && T = 0 \quad \text{on } x = 0,\\ &p = R(y - 1/2), && T = 1 \quad \text{on } x = L,\\ &v = 0, && \partial T/\partial y = 0 \quad \text{on } y = 0, 1. \end{aligned}\right\} \tag{5}$$

Here $R = \beta g h \kappa (T_h - T_c)/\nu\alpha$ is the Rayleigh number, $P = \kappa(p_h - p_c)/\mu\alpha$ is the dimensionless mean pressure difference, equivalent to the Peclet number (p_h and p_c are the hot-side and cold-side dimensional mean pressures), and $L = l/h$ is the aspect ratio. The symbols $\beta, g, \kappa, \nu, \alpha$ and μ are the coefficient of thermal expansion, gravitational acceleration, permeability, kinematic viscosity, effective thermal diffusivity and absolute viscosity, respectively. In the above equations the variables are nondimensionalized by defining

$$\left.\begin{aligned} &x, y = (x', y')/h; \quad u, v = (u', v')h/\alpha;\\ &p = [p' - p_h + \rho_c g(y' - h/2)](\mu\alpha/\kappa);\\ &T = (T' - T_c)/(T_h - T_c), \end{aligned}\right\} \tag{6}$$

where primes denote the dimensional variables, x' and y' are horizontal and vertical distances, u' and v' are

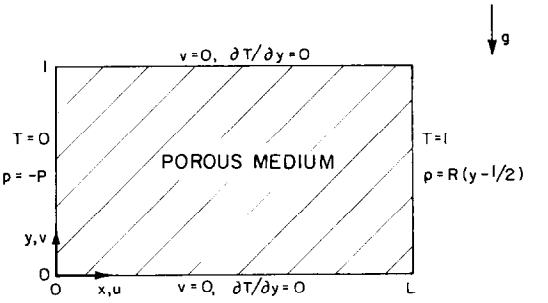

FIG. 1. Schematic of the 2-D horizontal porous channel.

Darcy velocity components in the x' and y' directions, p' and T' are pressure and temperature and ρ_c is the cold reservoir fluid density.

The dimensionless stream function is defined as

$$\psi = \int_0^y u \, dy. \tag{7}$$

The value of ψ on $y = 1$ is equal to the magnitude of the throughflow rate $\dot{m}$. From equations (2), (5) and (7) the relation between $\dot{m}$ and P can be easily found as

$$\dot{m} = -P/L. \tag{8}$$

It is also plausible to define a new dimensionless parameter ϕ, which represents the relative importance of the forced flow with respect to the buoyancy-driven flow, as

$$\phi = P/R. \tag{9}$$

Thus ϕ is a dimensionless end-to-end mean pressure difference scaled by R.

Finally, the nondimensional energy transfer through any cross section is given by the Nusselt number

$$N = L\int_0^1 (\partial T/\partial x - uT)\, dy. \tag{10}$$

The average temperature gradients at the cold-side and hot-side boundaries can be found to be

$$N_c = N; \quad N_h = N - P, \tag{11}$$

where

$$N_c = L\int_0^1 (\partial T/\partial x)_{x=0}\, dy; \quad N_h = L\int_0^1 (\partial T/\partial x)_{x=L}\, dy. \tag{12}$$

Therefore, the Nusselt number as defined by equation (10) is a measure of the mean horizontal temperature gradient at the cold boundary and the difference of the hot boundary mean temperature gradient and the total enthalpy transfer between the two reservoirs. For zero throughflow, $P = 0$, hence $N_h = N_c = N$.

For fixed R and L it can be shown that

$$T(L-x, 1-y, -P) = 1 - T(x, y, P), \tag{13a}$$

$$u(L-x, 1-y, -P) = -u(x, y, P), \tag{13b}$$

$$v(L-x, 1-y, -P) = -v(x, y, P), \tag{13c}$$

$$p(L-x, 1-y, -P) = p(x, y, P) - R(y-1/2) + P, \tag{13d}$$

$$N(-P) = N_h(P). \tag{13e}$$

Owing to this property of the solutions, only the case $P \geqslant 0$ is considered in this work, i.e. the throughflow direction is toward the cold reservoir.

3. LOW RAYLEIGH NUMBER SOLUTION

Regular perturbation solutions for this problem can be obtained by expanding the dependent variables u, v, p, T and ψ in a power series of R, i.e.

$$Q(x, y, R) = \sum_{i=0}^{\infty} R^i Q^{(i)}(x, y), \tag{14}$$

where Q stands for any of the dependent variables u, v, etc. and $Q^{(i)}$ which stands for $u^{(i)}$, $v^{(i)}$, etc. are perturbation functions to be determined. In order to study the range in which the driving forces for pressure and temperature driven flows are of the same order, it is assumed that $P = O(R)$ ($\phi = O(1)$). It can be easily shown that

$$u^{(0)} = v^{(0)} = p^{(0)} = \psi^{(0)} = 0; \quad T^{(0)} = x/L. \tag{15}$$

Consequently, the governing equations for $O(R)$ become

$$\left.\begin{aligned} &\partial u^{(1)}/\partial x + \partial v^{(1)}/\partial y = 0; \quad u^{(1)} = -\partial p^{(1)}/\partial x, \\ &v^{(1)} = -\partial p^{(1)}/\partial y + x/L; \\ &\partial^2 T^{(1)}/\partial x^2 + \partial^2 T^{(1)}/\partial y^2 = u^{(1)}/L, \\ &p^{(1)} = -\phi, \quad T^{(1)} = 0 \quad \text{on } x = 0, \\ &p^{(1)} = (y - 1/2), \quad T^{(1)} = 0 \quad \text{on } x = L, \\ &v^{(1)} = 0, \quad \partial T^{(1)}/\partial y = 0 \quad \text{on } y = 0, 1, \end{aligned}\right\} \tag{16}$$

the solutions for which can be obtained by noting that the horizontal velocity should be a superposition of a uniform throughflow, $-\phi/L$, induced by the end-to-end pressure difference, and a natural counterflow, $(1/2-y)/L$, imposed by the horizontal temperature gradient, thus

$$v^{(1)} = 0, \tag{17a}$$

$$u^{(1)} = \{-\phi/L\} + \{(1/2-y)/L\}, \tag{17b}$$

$$p^{(1)} = \{\phi(x/L-1)\} + \{x(y-1/2)/L\}, \tag{17c}$$

$$T^{(1)} = \{\phi x(L-x)/2L^2\} + \frac{1}{L^2}\left\{y^2/4 - y^3/6 - 1/24 + \frac{4}{\pi^4} \times \sum_{n=0}^{\infty} \frac{\sinh(2n+1)\pi x + \sinh(2n+1)\pi(L-x)}{(2n+1)^4 \sinh(2n+1)\pi L} \times \cos(2n+1)\pi y\right\}. \tag{17d}$$

In equations (17b)–(17d), the first groups are generated by the throughflow and the second groups are caused solely by the differential heating. Thus, up to $O(R)$, forced and natural convection act independently. Knowledge of the solutions thus far allows the determination of the Nusselt number up to $O(R^2)$. The problem for $T^{(2)}$ is

$$\nabla^2 T^{(2)} = u^{(1)}\partial T^{(1)}/\partial x + u^{(2)}/L, \tag{18a}$$

$$T^{(2)} = 0 \text{ on } x = 0, L; \quad \partial T^{(2)}/\partial y = 0 \text{ on } y = 0, 1. \tag{18b}$$

Integrating equation (18a) from 0 to 1 with respect to y using equations (17a)–(17d) and (18b) and the fact that

$$\int_0^1 u^{(2)}\, dy = 0,$$

then integrating with respect to x, one obtains

$$\int_0^1 (\partial T^{(2)}/\partial x)_{x=0}\,\mathrm{d}y = (1/120\,L^3)+\left[\phi^2/12-(16/L^3\pi^7)\times\sum_{n=0}^{\infty}(2n+1)^{-7}\tanh(n+1/2)\pi L\right]\Big/L. \quad (18c)$$

Using the expansion for the Nusselt number, one can derive a closed-form solution for N up to $O(R^2)$ as

$$N = 1+P/2+P^2/12+(R/L)^2\left[(1/120)-(16/\pi^7 L)\times\sum_{n=0}^{\infty}(2n+1)^{-7}\tanh(n+1/2)\pi L\right]+O(R^3), \quad (19)$$

with $P = O(R)$. The series in equations (17d), (18c) and (19) converge rapidly, so that replacing them by their leading terms gives excellent approximations for all practical purposes.

Although the non-linear interaction between the forced flow field and the natural convective field manifests itself in the expression for $T^{(2)}$ through the source term $u^{(1)}\,\partial T^{(1)}/\partial x$, the above equations indicate that up to $O(R^2)$ the contribution of each field to the heat transfer across the channel is independent of the other field. This is due to the fact that buoyancy-driven parts of the first-order horizontal velocity and temperature gradients are anti-symmetric functions of the distance from the channel centerline, while the corresponding forced convective parts do not depend on y, thus they are symmetric functions of this distance. Consequently, the interactive advection contributions to the heat transfer above and below the channel centerline cancel out.

4. LONG CHANNEL SOLUTION

This section deals with the effect of small throughflow rates on the natural convection in a porous channel for a situation where the Rayleigh number is fixed and the channel is long. In order to study the range in which the forced and natural convection contribution to the net heat transfer are of the same order, it is assumed that $P = \omega/L$ where $\omega = O(1)$. Here the treatment is similar in some respects to that given by Walker and Homsy [9] for the natural convection in a confined porous cavity. In the limiting case of $L\to\infty$, outer solutions for the problem valid in the core region, $O(L)$, can be obtained by regular expansion in $1/L$. These solutions, however, are not uniformly valid and break down in the end (inner) regions, the regions near the vertical walls with dimensionless length $O(1)$, where the flow should submit to the reservoirs' conditions. The existence of these two distinctive regions suggests a matched asymptotic expansion in the inverse of aspect ratio $(1/L)$.

4.1. *The core flow*

The scalings in the core region are taken to be

$$\bar{x} = x/L;\quad \bar{y} = y;\quad \bar{u} = uL;\quad \bar{v} = vL^2;\quad \bar{p} = p;\quad \bar{T} = T, \quad (20)$$

with these scalings, the governing field equations become

$$\partial\bar{u}/\partial\bar{x}+\partial\bar{v}/\partial y = 0, \quad (21)$$

$$\bar{u} = -\partial\bar{p}/\partial\bar{x}, \quad (22)$$

$$\bar{v} = L^2(R\bar{T}-\partial\bar{p}/\partial y), \quad (23)$$

$$\bar{u}\,\partial\bar{T}/\partial\bar{x}+\bar{v}\,\partial\bar{T}/\partial y = \partial^2\bar{T}/\partial\bar{x}^2+L^2\,\partial^2\bar{T}/\partial y^2, \quad (24)$$

$$\int_0^1 \bar{u}\,\mathrm{d}y = -P, \quad (25)$$

subject to the boundary conditions

$$R\bar{T} = \partial\bar{p}/\partial y(\bar{v}=0),\quad \partial\bar{T}/\partial y = 0 \quad \text{on} \quad y = 0,1, \quad (26)$$

and matching conditions (41) to be determined later.

The systematic asymptotic solutions for the core variables as a regular expansion in $(1/L)$ can be obtained by substituting the expansions of the core variables in terms of $(1/L)$ into equations (21)–(26) and equating terms of like power in $(1/L)$. The core region solutions expressed as asymptotic expansions in $(1/L)$ are

$$\bar{Q}(x,y,L) = \sum_{i=0}^{\infty}\bar{Q}_i(x,y)/L^i, \quad (27)$$

where $\bar{Q}$ stands for any of the core dependent variables $\bar{u}$, $\bar{v}$, etc. and $\bar{Q}_i$ which stands for $\bar{u}_i$, $\bar{v}_i$, etc. are perturbation functions in the core region to be determined.

The equations for $O(1)$ are

$$\left.\begin{aligned}&\partial\bar{u}_0/\partial\bar{x}+\partial\bar{v}_0/\partial y = 0;\quad \bar{u}_0 = -\partial\bar{p}_0/\partial\bar{x};\\ &R\bar{T}_0 = \partial\bar{p}_0/\partial y;\\ &\partial^2\bar{T}_0/\partial y^2 = 0;\quad \int_0^1\bar{u}_0\,\mathrm{d}y = 0;\\ &\partial\bar{T}_0/\partial y = 0 \text{ on } y = 0,1.\end{aligned}\right\} \quad (28a)$$

The solutions for this problem are

$$\bar{T}_0 = \bar{T}_0(\bar{x});\quad \bar{u}_0 = R(1/2-y)\,\mathrm{d}\bar{T}_0/\mathrm{d}\bar{x}. \quad (28b)$$

The unknown $\bar{T}_0(x)$ can be found by considering the $O(1/L^2)$ energy equation

$$\partial^2\bar{T}_2/\partial y^2 = \bar{u}_0\,\partial\bar{T}_0/\partial\bar{x}+\bar{v}_0\,\partial\bar{T}_0/\partial y-\partial^2\bar{T}_0/\partial\bar{x}^2, \quad (29a)$$

$$\partial\bar{T}_2/\partial y = 0 \quad \text{on } y = 0,1. \quad (29b)$$

Integrating equation (29a) and using equations (28b) and the boundary conditions (29b) yield

$$\mathrm{d}^2\bar{T}_0/\mathrm{d}\bar{x}^2 = 0, \quad (30)$$

and consequently

$$\left.\begin{aligned}&\bar{T}_0 = C_0\bar{x}+D_0;\quad \bar{u}_0 = RC_0(1/2-y);\quad \bar{v}_0 = 0,\\ &\bar{p}_0 = R(C_0\bar{x}+D_0)(y-1/2).\end{aligned}\right\} \quad (31)$$

By the same procedure the solutions up to any arbitrary order can be obtained. The solutions for

$O(1/L)$ are

$$\left.\begin{aligned}\bar{T}_1 &= C_1\bar{x}+D_1-\omega C_0\bar{x}^2/2,\\ \bar{u}_1 &= R(C_1-\omega C_0\bar{x})(1/2-y)-\omega,\\ \bar{v}_1 &= R\omega C_0(y-y^2)/2,\\ \bar{p}_1 &= R(C_1\bar{x}+D_1-\omega C_0\bar{x}^2/2)(y-1/2)+\omega(\bar{x}-1).\end{aligned}\right\} \quad (32)$$

By considering equations (5), one may notice that for $C_0 = 1$, $D_0 = 0$, $C_1 = \omega/2$ and $D_1 = 0$, equations (31) and (32) become uniformly valid, since they satisfy the $O(1)$ and $O(1/L)$ boundary conditions on $\bar{x} = 0, 1$. The second-order solutions are given by

$$\left.\begin{aligned}\bar{T}_2 &= C_2\bar{x}+D_2+\omega^2(\bar{x}^3/6-\bar{x}^2/4)\\ &\quad +R(y^2/4-y^3/6-1/24),\\ \bar{u}_2 &= R[C_2+\omega^2(\bar{x}^2-\bar{x})/2](1/2-y),\\ \bar{v}_2 &= R\omega^2(1/2-\bar{x})(y-y^2)/2,\\ \bar{p}_2 &= R[C_2\bar{x}+D_2+\omega^2(\bar{x}^3/6-\bar{x}^2/4)](y-1/2)\\ &\quad +R^2(2y^3-y^4-y+1/5)/24.\end{aligned}\right\} \quad (33)$$

Finally, the solution for $\bar{T}_3$ is

$$\bar{T}_3 = C_3\bar{x}+D_3+\omega(R^2/40-C_2)\bar{x}^2/2+\omega^3(2\bar{x}^3-\bar{x}^4)/24 +R\omega(1-2\bar{x})(y^2/4-y^3/6-1/24). \quad (34)$$

It can be easily perceived that equations (33) and (34) are not uniformly valid, therefore they should be corrected in the end regions. The details of these end-region flows, along with the matching conditions for each order yield the unknown constants C_i and D_i for $i \geqslant 2$.

4.2. *Flow in the end regions*

For the end regions, where the core flow communicates with the reservoirs, the transformations of the x-coordinate are taken as

$$\tilde{x} = x = L\bar{x}; \quad \hat{x} = L-x = L(1-\bar{x}), \quad (35)$$

where $\tilde{}$ and $\hat{}$ indicate the end-region variables at $x = 0$ and L, respectively. The governing equations for the cold-end region become

$$L\,\partial\tilde{u}/\partial\tilde{x}+\partial\tilde{v}/\partial y = 0, \quad (36)$$

$$\tilde{u} = -L\,\partial\tilde{p}/\partial\tilde{x}, \quad (37)$$

$$\tilde{v} = L^2(R\tilde{T}-\partial\tilde{p}/\partial y), \quad (38)$$

$$L\tilde{u}\,\partial\tilde{T}/\partial\tilde{x}+\tilde{v}\,\partial\tilde{T}/\partial y = L^2(\partial^2\tilde{T}/\partial\tilde{x}^2+\partial^2\tilde{T}/\partial y^2), \quad (39)$$

subject to the boundary conditions

$$\left.\begin{aligned}\tilde{p} = -P, \quad \tilde{T} = 0 \quad &\text{on } \tilde{x} = 0,\\ \partial\tilde{p}/\partial y = R\tilde{T}, \quad \partial\tilde{T}/\partial y = 0 \quad &\text{on } y = 0, 1,\end{aligned}\right\} \quad (40)$$

and the matching conditions

$$\lim_{\tilde{x}\to\infty}\tilde{Q}(\tilde{x}, y) = \lim_{\bar{x}\to 0}\bar{Q}(\bar{x}, y) = Q^*(\tilde{x}, y), \quad (41)$$

where Q stands for any of the dependent variables u, v, etc. and Q^* is the core dependent variable in terms of $\tilde{x}$.

As in the core region, the end-region solutions can be obtained as regular expansions in $(1/L)$ of the form

$$\tilde{Q}(\tilde{x}, y, L) = \sum_{i=0}^{\infty}\tilde{Q}_i(\tilde{x}, y)/L^i. \quad (42)$$

The first two temperature and pressure functions may be obtained by expanding $T^*(\tilde{x}, y)$ and $p^*(\tilde{x}, y)$ and taking the $O(1)$ and $O(1/L)$ terms, so

$$\left.\begin{aligned}\tilde{T}_0 = 0; \quad \tilde{T}_1 = \tilde{x}; \quad \tilde{p}_0 = 0;\\ \tilde{p}_1 = R\tilde{x}(y-1/2)-\omega,\end{aligned}\right\} \quad (43)$$

and consequently

$$\tilde{u}_0 = R(1/2-y). \quad (44)$$

In the light of the above solutions, the problem for $\tilde{T}_2$ can be written as

$$\partial^2\tilde{T}_2/\partial\tilde{x}^2+\partial^2\tilde{T}_2/\partial y^2 = R(1/2-y), \quad (45a)$$

$$\tilde{T}_2 = 0 \text{ on } \tilde{x} = 0; \quad \partial\tilde{T}_2/\partial y = 0 \text{ on } y = 0, 1, \quad (45b)$$

$$\lim_{\tilde{x}\to\infty}\tilde{T}_2 = D_2+\omega\tilde{x}/2+R(y^2/4-y^3/6-1/24). \quad (45c)$$

The solution for $\tilde{T}_2$ can be obtained as [10]

$$\tilde{T}_2 = \omega\tilde{x}/2+R\left[\frac{y^2}{4}-\frac{y^3}{6}-\frac{1}{24} +\frac{4}{\pi^4}\sum_{n=0}^{\infty}\frac{\cos(2n+1)\pi y\ \mathrm{e}^{-(2n+1)\pi\tilde{x}}}{(2n+1)^4}\right], \quad (46)$$

which yields $D_2 = 0$. By using equation (13a) the corresponding hot end-region solutions can be obtained. In particular C_2 can be evaluated from the $\hat{T}_2$ solution as $C_2 = \omega^2/12$.

Finally, the two unknown constants C_3 and D_3 may be determined by considering the problem for $\tilde{T}_3$ which is

$$\frac{\partial^2\tilde{T}_3}{\partial\tilde{x}^2}+\frac{\partial^2\tilde{T}_3}{\partial y^2} = R(y-1/2)\left[-\frac{\omega}{2} +\frac{4R}{\pi^3}\sum_{n=0}^{\infty}\frac{\cos(2n+1)\pi y\ \mathrm{e}^{-(2n+1)\pi\tilde{x}}}{(2n+1)^3}\right]+\tilde{u}_1, \quad (47a)$$

$$\tilde{T}_3 = 0 \text{ on } \tilde{x} = 0; \quad \partial\tilde{T}_3/\partial y = 0 \text{ on } y = 0, 1, \quad (47b)$$

$$\lim_{\tilde{x}\to\infty}\tilde{T}_3 = \omega^2\tilde{x}/12+D_3-\omega\tilde{x}^2/2 +R\omega(y^2/4-y^3/6-1/24). \quad (47c)$$

Integrating equation (47a) with respect to y, noting that

$$\int_0^1\tilde{u}_1\,\mathrm{d}y = -\omega$$

and using equation (47b), then integrating two times with respect to $\tilde{x}$ yield

$$\int_0^1\tilde{T}_3\,\mathrm{d}y = (8R^2/\pi^7)\sum_{n=0}^{\infty}[1-\mathrm{e}^{-(2n+1)\pi\tilde{x}}]/(2n+1)^7 -\omega\tilde{x}^2/2+a\tilde{x}. \quad (48)$$

Comparing the above equation with the corresponding expression obtained from equation (47c) one can show that $D_3 = 8R^2S\pi^7$ and $a = \omega^2/12$; similarly, from the $\hat{T}_3$ solution it can be shown that $C_3 = -16R^2S/\pi^7 - R^2\omega/80$, where S is formally obtained as

$$\sum_{n=0}^{\infty} (2n+1)^{-7},$$

but for all practical purposes, it can be taken as one.

It is difficult to proceed analytically beyond C_3 since the algebra becomes cumbersome. Substitution of the core solutions into equation (10) yields an asymptotic expansion for the Nusselt number valid for $L \to \infty$ with fixed R and $P = O(1/L)$ as

$$N = 1 + P/2 + P^2/12 + R^2(1/120 - 16S/\pi^7 L)/L^2 + O(1/L^4). \quad (49)$$

Note that in this case, also, the contributions of the forced flow and the natural convective flow to the heat transfer across the channel, up to $O(1/L^3)$, can be simply added, in spite of the non-linear interaction of the two fields which appears in the field variables.

The first-order corrections for the end-region velocity can be found as

$$\tilde{u}_1 = R^2\left\{\sum_{n=0}^{\infty}\left[\frac{2\sin(2n+1)\pi y}{(2n+1)^4\pi^4} + \frac{(2y-1)\cos(2n+1)\pi y}{(2n+1)^3\pi^3}\right]e^{-(2n+1)\pi\tilde{x}} + (3/8\pi^3)\sum_{m=1}^{\infty}\cos 2m\pi y\, e^{-2m\pi\tilde{x}}/m^3\right\} - \omega[1 + R(y-1/2)/2]. \quad (50)$$

Owing to the rapid convergence, replacing the series in equations (46), (47) and (50) by their leading terms gives excellent approximations. The corresponding hot-end region velocity, $\hat{u}_1$, can be obtained by using equation (13b).

5. NUMERICAL SOLUTIONS

To obtain the numerical solution to the governing equations [equations (1)–(4)], finite-difference schemes were used. Since the boundary conditions on $x = 0, L$ are prescribed for pressure, the velocity components can be eliminated from these equations, resulting in a Poisson equation for pressure as follows

$$\frac{\partial^2 p}{\partial x^2} + \frac{\partial^2 p}{\partial y^2} = R\frac{\partial T}{\partial y}. \quad (51)$$

This equation is coupled with the energy equation through the source term, therefore they should be solved simultaneously. To achieve this, the finite-difference form of these two equations along with the boundary conditions (5) were solved by the successive over-relaxation method. The computation was accomplished by a CDC 7600 computer, exploiting central-difference forms of the governing equations and second-order accurate forms of the boundary conditions.

The procedure was as follows: (1) the temperature T was initialized to its conduction value, equation (15), while the pressure p and velocities u and v were initialized to their first-order values, equations (17a)–(17c); (2) new temperature values were calculated from the central-difference form of the energy equation; (3) new boundary temperature values were computed on the horizontal boundaries; (4) having the temperature field, new pressure values were calculated from the central-difference form of the pressure equation, equation (51); (5) new boundary pressure values were computed on the horizontal boundaries; (6) having the pressure field, new velocity values were calculated; (7) the Nusselt number was evaluated from the obtained field; (8) steps 2–7 were repeated until final convergence. Stream function values were reckoned from the converged field. The solutions were assumed to be converged to the 'steady state' solutions when the following convergence criteria were all met

$$|T_{new} - T_{old}|_{max} \leqslant \varepsilon, \quad (52a)$$

$$|u_{new} - u_{old}|_{max} \leqslant \delta, \quad (52b)$$

$$|N_{new} - N_{old}| \leqslant \sigma, \quad (52c)$$

where 'max' denotes the maximum value over all the grid points. To achieve acceptable convergence, the values for ε, δ and σ were taken to be 10^{-4}, 10^{-3} and 10^{-4}, respectively. Since the non-conservative central-difference form of the equations were employed, the maximum deviation of the stream function values on the top horizontal boundary grid points from the theoretical value obtained by equation (8) serves as a criterion for both convergence and accuracy. Runs for which this maximum deviation was more than 2% of the maximum stream function value were rejected as being inaccurate. The accuracy of the scheme was also determined by decreasing the grid spacing and observing the change in the value of the Nusselt number. The grid spacing was decreased until less than a 2% change was observed in the Nusselt number.

The optimum relaxation parameter for T and p were found to be 1.45 and 1.8, respectively. Typically a high R run with a non-uniform grid of 81×51 points took between 1000 and 2000 iterations to converge and between 100 and 200 computing seconds on a CDC-7600 computer.

6. NUMERICAL RESULTS AND DISCUSSION

For the case of no throughflow, buoyancy driven flow is the only mode of convective motion. Since the effect of throughflow on this basic flow structure is under consideration, it is plausible to discuss this special case first.

6.1. *Zero net throughflow*

All calculations for this case were performed for values of R ranging up to 80 and for four different aspect ratios, $L = 2$, 3, 4 and 5.

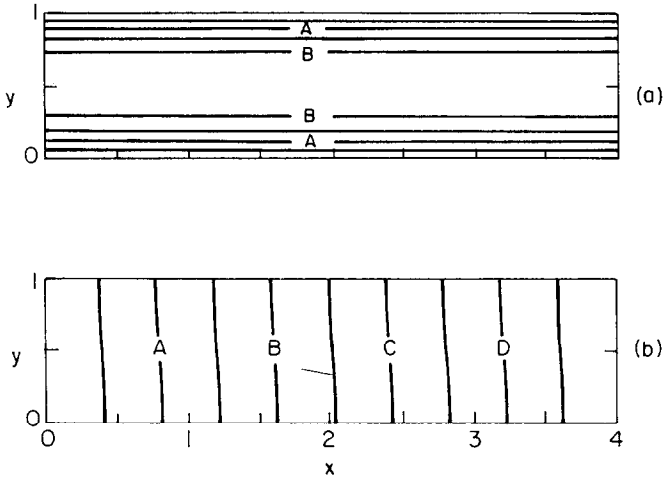

FIG. 2. Streamlines and isotherms for a case with $\phi = 0$, $R = 5$, $L = 4$. (a) Streamlines: $A = 0.03$; $B = 0.13$. (b) Isotherms: $A = 0.2$; $B = 0.4$; $C = 0.6$; $D = 0.8$.

In Figs. 2–4 typical streamlines and isotherms are plotted for different values of L and R. Since for this case the net throughflow is zero ($\phi = P = 0$) the flow fields are centro-symmetric. The flow in the core region is parallel to the top and bottom walls of the channel which is in agreement with the asymptotic solutions. In this regime, effectively all of the temperature drop occurs along the core and the temperature weakly depends on y. This confirms the asymptotic results which indicate that to the first order T is independent of vertical position and varies linearly between the vertical boundaries. The constant temperature gradient in the core is solely responsible for the fluid motion.

In the end regions, the flow structure deviates from parallel flow and this deviation becomes more significant as R increases or L decreases. For $R = 5$ and $L = 4$ this deviation is quite negligible (Fig. 2). This can be explained by the analytical results which indicate that for small R or large L the core parallel flow solution is uniformly valid to the first order. On the other hand, for $R = 50$ and $L = 5$ the deviation is quite remarkable (Fig. 4). The reason is that the non-linearity for this case is sufficiently strong and the higher order corrections are not negligible anymore. For $R = 20$ and $L = 5$ the deviation is small but perceptible (Fig. 3).

For high enough R (or small enough L), a recirculating flow occurs in the cold-end region, i.e. a portion of the cold fluid, which recharges from the lower part of the permeable boundary, discharges from the upper part of the same boundary. Similar behavior is shown by the hot-end region, but owing to the centro-symmetry, only the cold-end region is discussed here. This non-linear behavior can be explained as follows: the horizontal temperature gradient establishes the parallel flow in the core. In this region the flow is fully developed, i.e. $u = u(y)$ and $\partial T/\partial x = f(y)$. Since at $x = 0$ the core flow should submit to constant reservoir temperature, in the upper part of the cold-end region

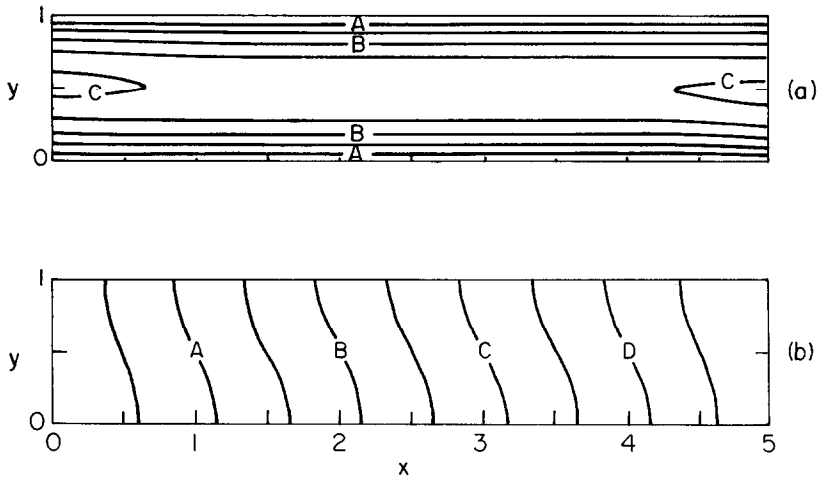

FIG. 3. Streamlines and isotherms for a case with $\phi = 0$, $R = 20$, $L = 5$. (a) Streamlines: $A = 0.1$; $B = 0.3$; $C = 0.5$. (b) Isotherms: $A = 0.2$; $B = 0.4$; $C = 0.6$; $D = 0.8$.

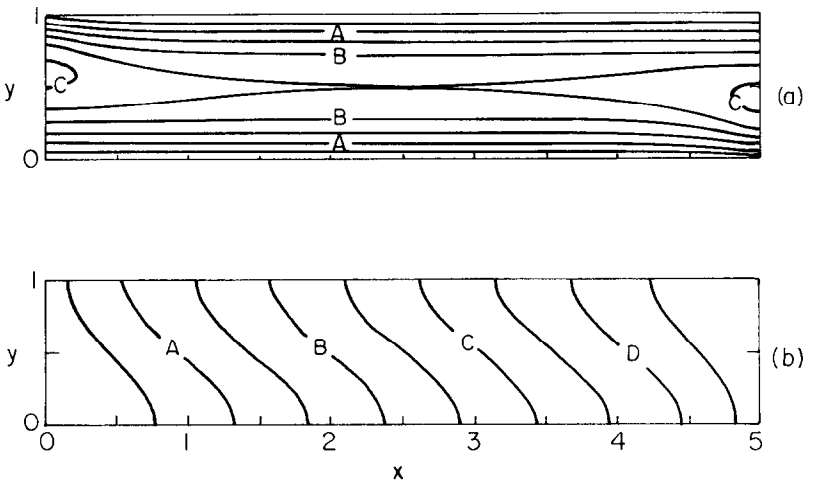

FIG. 4. Streamlines and isotherms for a case with $\phi = 0$, $R = 50$, $L = 5$. (a) Streamlines: $A = 0.48$; $B = 0.96$; $C = 1.43$. (b) Isotherms: $A = 0.2$; $B = 0.4$; $C = 0.6$; $D = 0.8$.

there should be a transition zone (discharge zone) where the isotherms are compressed. The compression of the isotherms causes a higher temperature gradient in this discharge zone. Consequently, the horizontal velocity, which is driven mainly by the horizontal temperature gradient, increases. The horizontal velocity distribution at the cold boundary for $R = 30$, 50 and $L = 5$ depicted on Fig. 6, along with the asymptotic results for long channels, indicates the above-mentioned behavior. As R increases, the core velocity augments, so the compression of isotherms becomes more intense; consequently the horizontal velocity in the discharge zone becomes even higher. Thus, since the fluid is incompressible, a recirculating flow comes about in order to satisfy continuity (Fig. 4).

As the Rayleigh number increases the dependence of the core temperature on vertical position becomes more significant; the recirculating flows penetrate further into the core and eventually meet at the middle of the channel $x = L/2$. In this way the parallel flow in the core disappears and the asymptotic solutions are not valid anymore. The above phenomenon has not been accounted for in Bejan and Tien's [1] approximate solutions.

The asymptotic core solutions in Section 4 for the case of no net mass flow become identical to those given in refs. [1, 9] and the Nusselt number can be evaluated from

$$N_a = N(P = 0)$$
$$= 1 + R^2(1/120 - 16S/\pi^7 L)/L^2 + O(1/L^4). \quad (53)$$

Note also that $\tanh \alpha \simeq 1$ for $\alpha \geqslant \pi$ ($\tanh \pi = 0.996$), therefore, the expression for the Nusselt number, equation (19), derived in Section 3 for $L \gtrsim 2$ and $P = 0$ becomes the same as equation (53). Thus, equation (53), as well as equation (48), are valid for $L \to \infty$ with fixed R, though arbitrary, as well as for $R \to 0$ with $L \gtrsim 2$.

From equation (53) and also from the first-order temperature distribution in Section 4, it is clear that for a long channel the dominated mode of heat transfer is conduction. As in the case of a confined porous cavity [9], the conduction dominance for a long channel with fixed R (though large), is a result of the cumulative effect of locally small Darcy's resistances acting over an adequately long distance and as $L \to \infty$ the damping force in the core becomes more responsible for establishing the flow structure for all fixed though large values of the Rayleigh number.

Figure 5 depicts the variation of the Nusselt number with the aspect ratio for different values of R along with the results of Bejan and Tien [1]. From this figure, it can be observed that the numerical results are in good agreement with the asymptotic solutions provided that the channel is not very short and the Rayleigh number not very large.

Figure 6 is a plot of the analytically and numerically determined horizontal velocity profiles on $x = 0$ as a function of y. It is observed that as R decreases the velocity profiles approach more closely to the corresponding asymptotic profiles. The behavior of the velocity distribution on $x = 0$ was explained earlier.

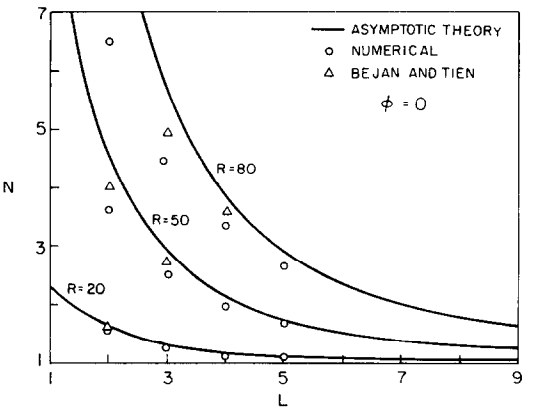

FIG. 5. Variation of the Nusselt number with the channel aspect ratio.

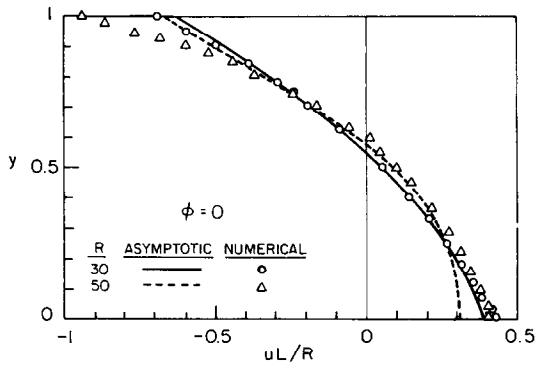

FIG. 6. Comparison of numerically determined horizontal velocity at $x = 0$ with the asymptotic results $(u = \tilde{u}_0/L + \tilde{u}_1/L^2)$.

Although Bejan and Tien [1] did not consider this type of behavior in the end region, the numerical heat transfer results obtained here are in good agreement with their results. This is due to the fact that the main resistance to the flow comes from the core and that the end regions in this range of parameters are dynamically passive. It should be mentioned that here the vertical boundaries are assumed to be maintained at constant temperatures, whereas in Bejan and Tien's [1] analysis, owing to the special treatment of the end regions, this assumption was relaxed. The comparison of the results shows that, for the range considered here, the effect of energy discharge through the vertical permeable boundaries is small, consequently, the assumption of constant temperature at the vertical boundaries is plausible.

6.2. *Throughflow effect*

In order to consider the throughflow effect on the natural convection, numerical results have been obtained for values of R ranging up to 80 for two different aspect ratios $L = 3$ and 5. The dimensionless pressure difference ϕ has been varied from 0 to 0.5.

Figures 7–12 present the streamlines and isotherms for different values of the Rayleigh number and the dimensionless mean pressure difference. As was mentioned earlier, owing to conditions (13), only positive values of ϕ are considered, i.e. the net mass flow (throughflow) is toward the cold reservoir ($\dot{m}$ is negative).

From Fig. 7 it can be seen that for small values of ϕ and R in a long channel ($\phi = 0.05$, $R = 5$ and $L = 5$), the flow is parallel all through the channel and temperature is linear with a negligible dependence on the vertical position y. In this case, the linear temperature gradient caused by conduction induces a natural counterflow with balanced streams, parallel to the top and bottom walls of the channel, whose magnitude is small and does not disturb the linear temperature field remarkably. Moreover, the small pressure difference induces a uniform flow which, due to its small magnitude, does not disturb the linear temperature field either. Thus, the two fields act independently and the superposition of these two causes a parallel flow (Fig. 7). In this situation, it can be concluded that the second-order correction is insignificant. This behavior is in agreement with the results of Section 3 which indicates that to the first order the temperature distribution is linear and for $P = O(R)$

$$u = [-P/L] + [R(1/2 - y)/L] + O(R^2), \quad (54)$$

where P/L is the magnitude of the uniform throughflow imposed by a mean pressure difference and $[R(1/2-y)/L]$ is the natural counterflow with balanced streams induced by a linear temperature gradient. The asymptotic expression for $\bar{u}$ in Section 4 can be rewritten as

$$u = \bar{u}/L = [-P/L] + [R(1/2-y)/L] - [RP(x/L - 1/2)(1/2-y)] + \text{H.O.T.}, \quad (55)$$

which up to the first order in R yields essentially the same expression as equation (54). The third group

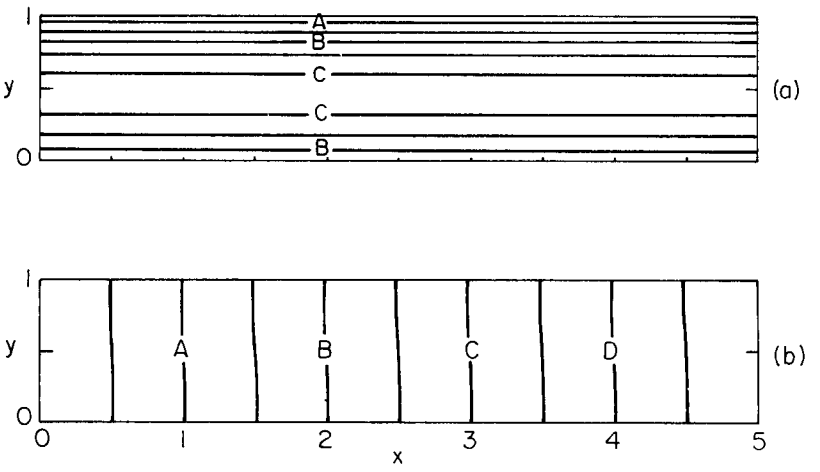

FIG. 7. Streamlines and isotherms for a case with $\phi = 0.05$, $R = 5$, $L = 5$. (a) Streamlines: $A = -0.02$; $B = 0.03$; $C = 0.09$. (b) Isotherms: $A = 0.2$; $B = 0.4$; $C = 0.6$; $D = 0.8$.

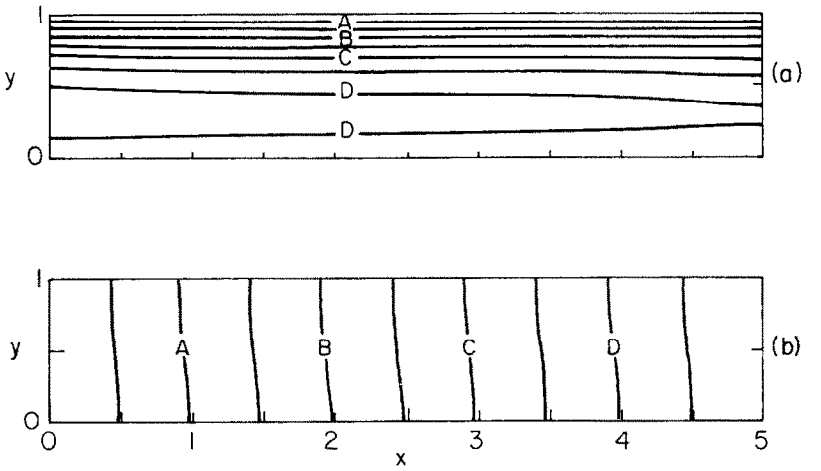

FIG. 8. Streamlines and isotherms for a case with $\phi = 0.2$, $R = 5$, $L = 5$. (a) Streamlines: $A = -0.16$; $B = -0.09$; $C = -0.03$; $D = 0.03$. (b) Isotherms: $A = 0.2$; $B = 0.4$; $C = 0.6$; $D = 0.8$.

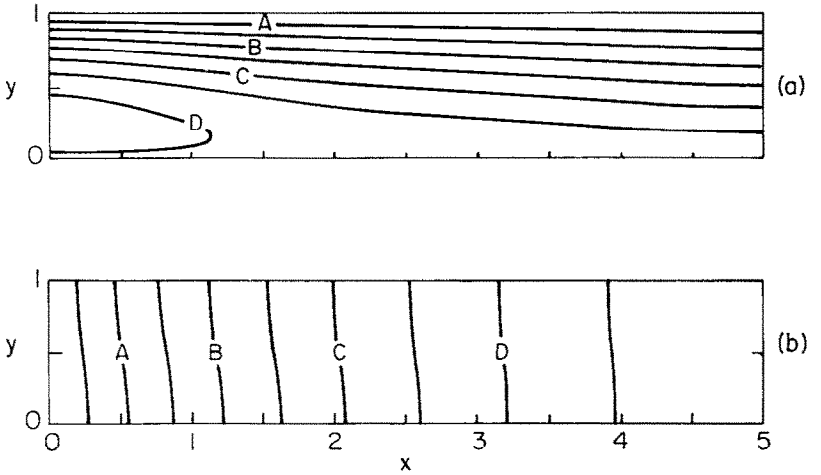

FIG. 9. Streamlines and isotherms for a case with $\phi = 0.5$, $R = 5$, $L = 5$. (a) Streamlines: $A = -0.42$; $B = 0.27$; $C = -0.13$; $D = 0.01$. (b) Isotherms: $A = 0.2$; $B = 0.4$; $C = 0.6$; $D = 0.8$.

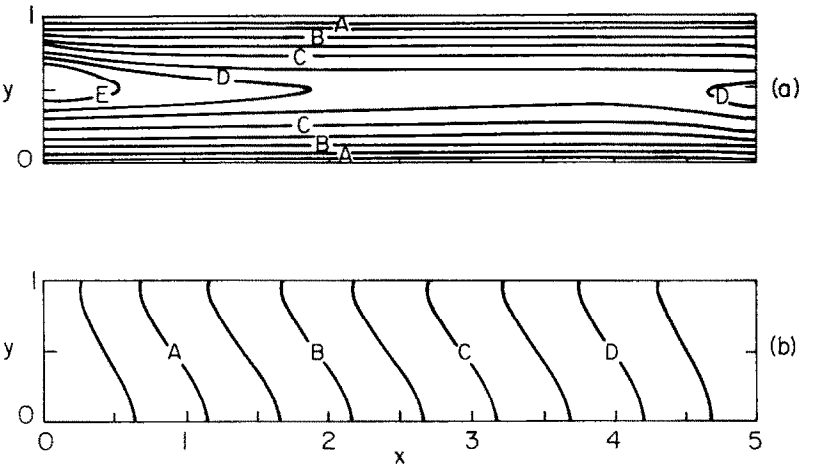

FIG. 10. Streamlines and isotherms for a case with $\phi = 0.01$, $R = 30$, $L = 5$. (a) Streamlines: $A = 0.05$; $B = 0.30$; $C = 0.53$; $D = 0.71$; $E = 0.77$. (b) Isotherms: $A = 0.2$; $B = 0.4$; $C = 0.6$; $D = 0.8$.

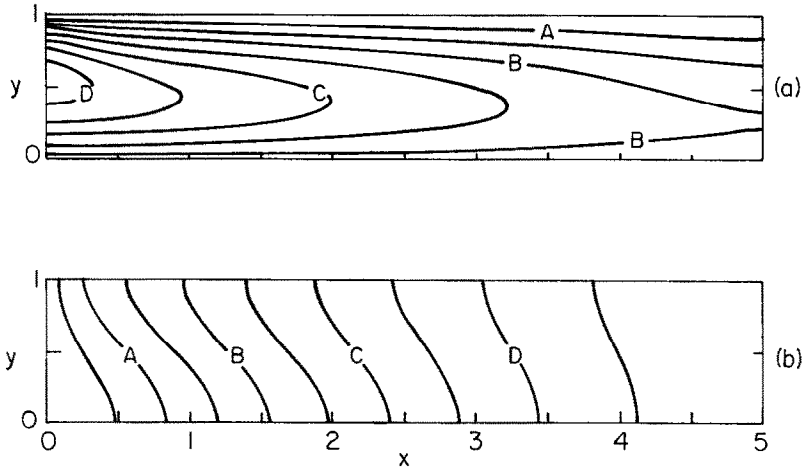

FIG. 11. Streamlines and isotherms for a case with $\phi = 0.1$, $R = 30$, $L = 5$. (a) Streamlines: $A = -0.34$; $B = 0.11$; $C = 0.55$; $D = 0.99$. (b) Isotherms: $A = 0.2$; $B = 0.4$; $C = 0.6$; $D = 0.8$.

in equation (55) is generated by interaction of the two flows.

For the same R and L as the pressure difference increases the throughflow rate also increases, the streamlines deviate from being parallel, the isotherms are more compressed toward the cold reservoir, the temperature dependence on the vertical position y is observable, though small, and a recirculating flow occurs at the cold boundary. In this case, as the throughflow passes from the hot side to the cold end, it compresses the isotherms toward the left. The temperature gradient caused by this compression augments both the recharge and discharge velocities near the cold end, thus the streamlines in the discharge zone become closer to the top and in the recharge zone closer to the bottom boundary.

The above-mentioned behavior is in concordance with the asymptotic results and equation (55), shows the same behavior as discussed above. Moreover, the vertical velocity component at the core region (Section 4) can be rewritten as

$$v = -\frac{RP}{2L^2}(y^2 - y)\left[1 - P\left(\frac{x}{L} - \frac{1}{2}\right)\right] + \text{H.O.T.}, \quad (56)$$

which indicates that for small pressure differences, $v \ll u$ (for $\phi = 0.05$, $v \simeq 0$, Fig. 7). For positive values of ϕ, the magnitude of v decreases linearly with x; near the hot-end region, v is inconsequential and gradually becomes significant as x decreases from L to zero. By increasing the pressure difference, higher vertical velocities ensue; consequently more of the thermally recharged flow reverses. For either $P = 0$ or $R = 0$, vertical velocity at the core vanishes, hence v seems to be a good indicator of the interaction between the two fields. Equation (56) indicates that for higher pressure differences, higher values of the Rayleigh number and lower aspect ratios, the interaction is more pronounced.

The core temperature derived in Section 4 can be

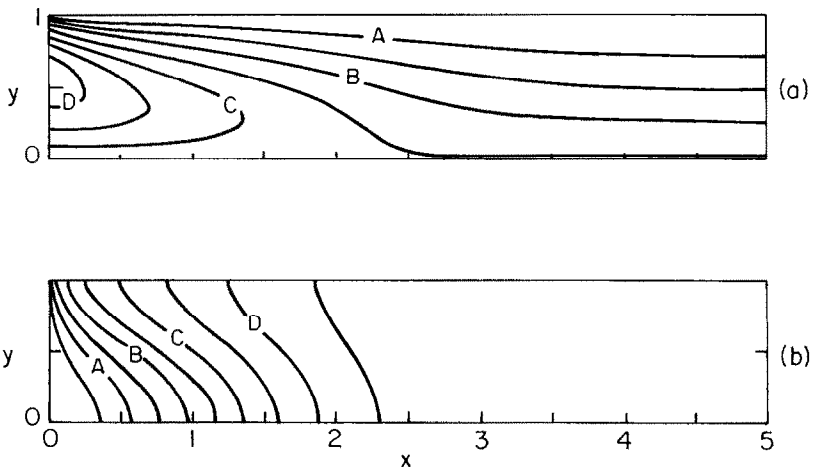

FIG. 12. Streamlines and isotherms for a case with $\phi = 0.35$, $R = 30$, $L = 5$. (a) Streamlines: $A = -1.52$; $B = -0.52$; $C = 0.48$; $D = 1.48$. (b) Isotherms: $A = 0.2$; $B = 0.4$; $C = 0.6$; $D = 0.8$.

rewritten as

$$\bar{T} = \left\{\bar{x}\left(1+\frac{P}{2}+\frac{P^2}{12}\right)-\frac{\bar{x}^2P}{2!}\left(1+\frac{P}{2}+\frac{P^2}{12}\right)+\frac{\bar{x}^3P^2}{3!}\left(1+\frac{P}{2}\right)-\frac{\bar{x}^4P^3}{4!}\right\}+\left\{\frac{R}{L^2}\left(\frac{y^2}{4}-\frac{y^3}{6}-\frac{1}{24}\right)-\frac{16SR^2}{\pi^7L^3}(\bar{x}-1/2)\right\}+\left\{\frac{RP}{L^2}\left[\left(\frac{y^2}{4}-\frac{y^3}{6}-\frac{1}{24}\right)(1-2\bar{x})+\frac{R\bar{x}}{80}(1-\bar{x})\right]\right\}+O(1/L^4). \quad (57)$$

The first group is simply the temperature distribution due to pure forced convection ($R = 0$) for small values of pressure difference. Its exact solution can be easily shown to be

$$T_f = (1-e^{-P\bar{x}})/(1-e^{-P}), \quad (58)$$

whose expansion for $|P| < 2\pi$ is exactly the first group in equation (57). Here f stands for forced convection. The second group is the temperature deviation from the state of pure conduction due to the thermally driven flow. Finally, the third group is caused by interaction between the two fields which vanishes as either P or R goes to zero. The first group in equation (57) as well as equation (58) show the compression of the isotherms toward the cold boundary for $P > 0$.

As the pressure difference increases more, the adverse pressure gradient makes a larger portion of the thermally recharged cold fluid to recirculate and eventually, all of it recirculates. For even higher pressure differences the recirculating flow will be confined in a smaller region near the cold end. In the hot-end vicinity, due to the high throughflow rate the temperature gradient becomes frivolous; thus, the natural convective motion vanishes and the flow becomes quite uniform. Conversely, due to the compression of the isotherms, natural convective motion does not vanish and recirculating flow does exist in the cold-end region.

Streamlines and isotherms for $R = 30$ and $L = 5$ are shown in Figs. 10–12 for different rates of throughflow. For $\phi = 0.01$, Fig. 10, the core streamlines are almost parallel and the flow field is a superposition of a uniform flow and a natural counterflow with balanced streams in accordance with equations (54) and (55). In the end regions the deviation from the parallel flow structure is not negligible anymore as it was in the previous case ($R = 5$, $L = 5$). Compression of isotherms due to the stronger thermally driven motion in the end region is responsible for this deviation. Obviously, the asymmetry of the end regions is due to the effect of throughflow on the isotherms since it decreases the hot-side compression and enhances the cold-end condensation of the isotherms. For $\phi = 0.1$ the hot-side recirculating flow vanishes (Fig. 11) and for $\phi = 0.35$ the flow is almost uniform in this region (Fig. 12). For $R = 80$ and $L = 5$ basically the same behavior is seen.

Next, consider the effect of the Rayleigh number variation on the flow field with fixed L and ϕ. As R increases the temperature gradient in the cold discharge zone becomes sharper, hence, the thermally driven motion becomes relatively more intense, cold fluid discharge velocity increases, and discharge area shrinks. On the other hand, the behavior of the flow near the hot boundary depends on the magnitude of ϕ. For $L = 3$ and $\phi = 0.1$ as R increases the natural convective motion becomes more pronounced, whereas for $\phi = 0.2$ increasing the Rayleigh number thwarts the natural convection in this region. Heat transfer enhancement by the thermally driven flow, which will be discussed later, shows the same trend as well (Fig. 14).

6.3. *Heat transfer results*

Figure 13 shows the variation of the Nusselt number with the mean pressure difference, ϕ, for $R = 30$ and aspect ratios of $L = 3$ and 5. For $\phi > 0.2$ the numerical results coincide with the forced-convection asymptote which can be easily shown to be

$$N_f = P/(1-e^{-P}) = 1+P/2+P^2/12-P^4/720+,\ldots \quad \text{for } |P| < 2\pi, \quad (59a)$$

or substituting for $P = \phi R$, N_f can be rewritten as

$$N_f = \phi R/(1-e^{-\phi R}), \quad (59b)$$

which is independent of L. Notice that for $\phi \gtrsim 0.13$ the forced-convection asymptote becomes a straight line. The reason is that for high throughflow rates the temperature gradient in the hot-end region becomes flat ($N_h = 0$), so from equation (11) one can obtain $N = P = \phi R$, which could also be deduced from equation (59). The above relation indicates that for this limit, the heat transfer is simply equal to the enthalpy change of the fluid being forced through the channel on a mass flow basis. On the other hand, for smaller values of ϕ the numerical results approach the asymptotic

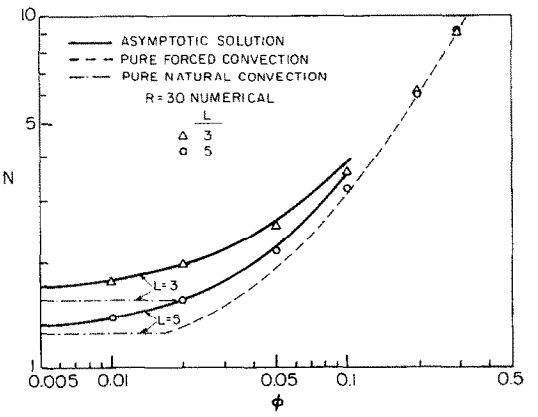

FIG. 13. Heat transfer variation with the throughflow rate.

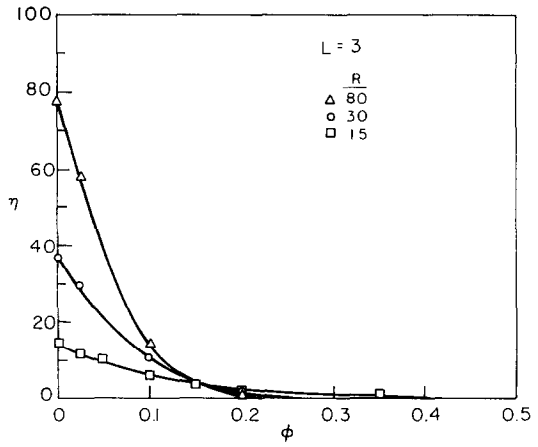

FIG. 14. Variation of the heat transfer enhancement due to the thermally driven flow with throughflow rate.

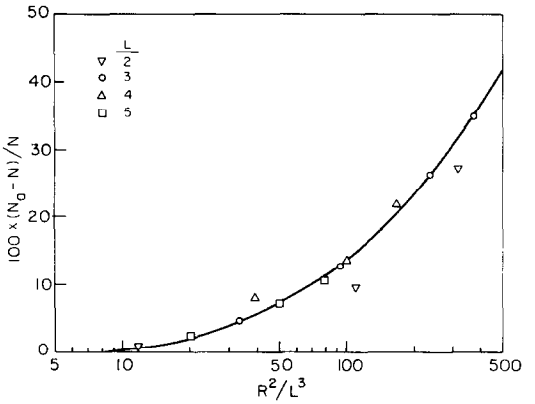

FIG. 15. Percentage deviation of the Nusselt number from its asymptotic value for zero net throughflow ($\phi = 0$), N_a is the asymptotic Nusselt number.

results indicated by the solid line. For all cases studied here the results show that the natural-convection contribution to the heat transfer is negligible for $\phi \gtrsim 0.2$. As $\phi \to 0$ both numerical and asymptotical results approach the pure natural-convection asymptote.

Heat transfer enhancement due to the thermally driven flow for $L = 3$ and $R = 15, 30$ and 80 is shown in Fig. 14. The enhancement is defined as

$$\eta = (N - N_f)/N. \tag{60}$$

It is seen that for small throughflow rates (small ϕ) the enhancement can be quite large, but as the throughflow rate increases it falls off quite quickly such that for $\phi \gtrsim 0.2$ it is relatively unimportant. For $\phi \lesssim 0.175$ as R increases, the enhancement becomes more significant, whereas for $\phi \gtrsim 0.175$ the converse is true. For channels of other aspect ratios the form of the curve is similar although the enhancement degree does depend on the aspect ratio and, as might be expected, it increases with decreasing L.

Finally, the parametric domain in which the asymptotic solutions are acceptable can be determined by noting that the $O(1)$ term in the Nusselt number results must be larger than higher order terms. Therefore

$$R^2/L^3 < \pi^7/16, \quad 120/L; \quad P = R\phi < 2.$$

Figure 15 shows the deviation of the asymptotic Nusselt number N_a, evaluated from equation (53), from the corresponding numerical result N, for different values of the parameter (R^2/L^3). It is seen that for $R^2/L^3 \leqslant 50$ this deviation is less than 7%. Moreover, Fig. 13 indicates that for $R = 30$ the asymptotic predictions are acceptable for values of the pressure differences below about $\phi = 0.05$, yielding $P = R\phi = 1.5$ as the upper bound of the validity range.

7. CONCLUDING REMARKS

The mechanism of flow and heat transfer by combined forced and natural convection through a 2-D horizontal porous channel has been studied both analytically and numerically. The results demonstrate the dependence of the Nusselt number on the aspect ratio of the channel, the Rayleigh number and dimensionless end-to-end mean pressure difference (equivalent of Peclet number) which is also a measure of the throughflow rate.

For low Rayleigh numbers, the effect of throughflow on the natural convection, induced by a horizontal temperature gradient, has been analyzed by the regular perturbation method, and closed-form solutions, valid for small values of (R^2/L^3) and P, have been obtained. Similar results have been derived for a long channel by the matched asymptotic expansions. For these limits, although the non-linear interaction between the forced throughflow and the thermally driven motion manifests itself in the temperature and velocity distributions, the results for the Nusselt number indicate that the contribution of the two fields to the heat transfer through the channel can be simply added. For the range where the asymptotic results break down, numerical solutions have been obtained. The results show also that, even a small throughflow rate plays an important role in re-distributing the temperature in the channel. For higher values of throughflow rate the natural convection is suppressed in the injection side and the Nusselt number approaches the forced-convection asymptote. The effects of the Rayleigh number and the aspect ratio variations on the role of natural convection are shown.

REFERENCES

1. A. Bejan and C. L. Tien, Natural convection in a horizontal porous medium subjected to an end-to-end temperature difference, *J. Heat Transfer* **100**, 191–198 (1978).
2. J. W. Elder, Steady free convection in a porous medium heated from below, *J. Fluid Mech.* **27**(1), 29–48 (1967).
3. M. Prats, The effect of horizontal fluid flow on thermally induced convection currents in porous mediums, *J. Geophys. Res.* **71**, 4835–4837 (1966).
4. M. A. Combarnous and P. Bia, Combined free and forced convection in porous media, *Soc. Petro. Engrs. Journal* **11**, 399–405 (1971).

5. G. M. Homsy and A. E. Sherwood, Convective instabilities in porous media with throughflow, *A.I.Ch.E. Jl* **22**, 168–174 (1976).
6. I. G. Donaldson, The simulation of geothermal systems with a simple convective model, *Geothermics* **2**, 649–654 (1970).
7. P. J. Burns, L. C. Chow and C. L. Tien, Convection in a vertical slot filled with porous insulation, *Int. J. Heat Mass Transfer* **20**, 919–926 (1977).
8. A. Bejan and J. Imberger, Heat transfer by forced and free convection in a horizontal channel with differentially heated ends, *J. Heat Transfer* **101**, 417–421 (1979).
9. K. L. Walker and G. M. Homsy, Convection in a porous cavity, *J. Fluid Mech.* **87**, 449–474 (1978).
10. M. Haajizadeh, Convection in horizontal porous media with different end temperatures, Ph.D. thesis, University of California, Berkeley, California (1982).

CONVECTION MIXTE DANS UN CANAL POREUX HORIZONTAL

Résumé — On étudie analytiquement et expérimentalement les écoulements mixtes à travers un canal poreux horizontal qui raccorde deux réservoirs. L'écoulement forcé est induit par une différence de pression entre les extrémités, tandis que le mouvement de convection naturelle est dû à un gradient de température horizontal. Les solutions sont gouvernées par trois paramètres adimensionnels: le nombre de Rayleigh R basé sur la perméabilité, le rapport de forme du canal L (longueur/hauteur) et la différence de pression sans dimension P, équivalent au nombre de Péclet. Pour les petits R, L fixé et $P = O(1)$, on établit une expression asymptotique basée sur l'analyse régulière de perturbation, pour un nombre de Nusselt jusqu'à $O(R^2)$ quand $R \to 0$. Pour R fixé et $P = O(1/L)$, des solutions pour des canaux longs sont trouvés en utilisant des développements asymptotiques, et le nombre de Nusselt est évalué jusqu'à $O(1/L^3)$. Enfin les solutions numériques des équations sont obtenues par une technique aux différences finies à sur-relaxation. Ces solutions couvrent le domaine $R \leqslant 80, 2 \leqslant L \leqslant 5$ et $0 \leqslant P/R \leqslant 0{,}5$. Une comparaison avec les solutions numériques montre que les solutions asymptotiques sont valables pour le domaine $(R^2/L^3) \leqslant 50$ et $P \leqslant 1{,}5$. Pour ce domaine, les résultats indiquent que les accroissements de transfert thermique dus à la convection naturelle et à l'écoulement forcé peuvent être simplement additionnés malgré l'interaction non linéaire de ces deux champs. Les résultats montrent aussi que même un petit débit a une influence sensible sur la distribution de température et de transfert thermique à travers le canal, et pour $P/R \geqslant 0{,}2$ la contribution de la convection naturelle au nombre de Nusselt est négligeable.

ÜBERLAGERTE FREIE UND ERZWUNGENE KONVEKTION IN EINEM HORIZONTALEN PORÖSEN KANAL

Zusammenfassung — In der vorliegenden Arbeit wurden überlagerte freie und erzwungene Konvektionsströmungen in einem horizontalen Kanal, der zwei Behälter miteinander verbindet, sowohl numerisch als auch analytisch untersucht. Der erzwungene Durchfluß wird durch eine mittlere Druckdifferenz an den Kanalenden erzeugt, während sich die freie Strömung durch einen Temperaturgradienten in horizontaler Richtung einstellt. Die Lösung wird hauptsächlich von drei dimensionslosen Parametern bestimmt: der Rayleigh-Zahl R, die von der Permeabilität abhängt, dem Verhältnis Kanallänge zu Kanalhöhe L und der dimensionslosen Druckdifferenz zwischen den Kanalenden P, die der Peclet-Zahl entspricht. Für kleine R, feste Werte von L und $P = O(1/L)$ kann eine asymptotische Lösung, die auf der Störungsrechnung basiert, für Nusselt-Zahlen bis zu $O(R^2)$, wenn R gegen null geht, gefunden werden. Für feste R und $P = O(1/L)$ wurden Lösungen für lange Kanäle ($L \to \infty$) ermittelt, indem angepaßte asymptotische Reihen verwendet werden, wobei die Nusselt-Zahl bis zu $O(1/L^3)$ berechnet wurde. Durch Anwendung eines Differenzenverfahrens mit sukzessiver Überrelaxation wurden die numerischen Lösungen der vollständigen Bestimmungsgleichungen erhalten. Diese Lösungen überdecken den Parameterbereich von $R \leqslant 80$, $2 \leqslant L \leqslant 5$ und $0 \leqslant P/R \leqslant 0{,}5$. Ein Vergleich mit den numerischen Lösungen zeigt, daß die asymptotischen Lösungen für den Parameterbereich von $(R^2/L^3 \lesssim 50$ und $P \lesssim 1{,}5$ gültig sind. In diesem Bereich weisen die Ergebnisse darauf hin, daß die anteiligen Zunahmen des Wärmetransports durch freie Konvektion und erzwungene Strömung einfach addiert werden können, und zwar ungeachtet der nicht-linearen Wechselwirkung dieser beiden Felder. Die Ergebnisse zeigen auch, daß schon ein kleiner Durchfluß einen bedeutenden Einfluß auf die Temperaturverteilung und den Wärmetransport quer zum Kanal hat und daß für $P/R \gtrsim 0{,}2$ der Einfluß der freien Konvektion auf die Nusselt-Zahl vernachlässigbar ist.

СОВМЕСТНАЯ ЕСТЕСТВЕННАЯ И ВЫНУЖДЕННАЯ КОНВЕКЦИЯ В ГОРИЗОНТАЛЬНОМ ПОРИСТОМ КАНАЛЕ

Аннотация—Аналитически и численно исследуется совместная естественная и вынужденная конвекция в горизонтальном пористом канале, соединяющем два резервуара. Вынужденное продольное течение вызывается разностью среднего давления на концах канала, а естественная конвекция происходит за счет горизонтального градиента температур. Решения определяются тремя безразмерными параметрами: числом Релея R, основанном на проницаемости, отношением размеров строн канала L (длина к высоте) и безразмерной разностью давления P на концах канала, эквивалентной числу Пекле. Для малого R, постоянного L и при $P = O(1)$ с помощью метода возмущений получено асимптотическое выражение для числа Нуссельта с точностью до $O(R^2)$ при $R \to 0$. Для постоянного R и $P = O(1/L)$ решения для каналов большой длины, $L \to \infty$, находятся методом сращиваемых асимптотических разложений, число Нуссельта рассчитывается с точностью до $O(1/L^3)$. Наконец, методом верхней релаксации получены численные решения конечно-разностных приближений полных уравнений для следующих диапазонов параметров: $R \leq 80$, $2 \leq L \leq 5$ и $0 \leq P/R \leq 0{,}5$. Сравнение с численными решениями показывает, что асимптотические решения справедливы при $(R^2/L^3) \lesssim 50$ и $P \lesssim 1{,}5$. В этих случаях, как следует из полученных результатов, увеличение теплопереноса за счет естественной и вынужденной конвекции может быть получено простым суммированием, несмотря на нелинейное взаимодействие между этими двумя полями. Результаты показывают также, что даже при небольшой скорости продольное течение оказывает большое влияние на распределение температуры и теплоперенос поперек канала, в то время как при $P/R \gtrsim 0{,}2$ естественная конвекция практически не влияет на число Нуссельта.